



**A General Structural Order Parameter for the Amorphous
Solidification of a Supercooled Liquid**

Gang Sun^{1,2} and Peter Harrowell^{1,*}

1, School of Chemistry, University of Sydney, Sydney New South Wales 2006, Australia

2, Department of Fundamental Engineering, Institute of Industrial Science, University of Tokyo, 4-6-1 Komaba, Meguro-ku, Tokyo 153-8505, Japan.

* Corresponding author: peter.harrowell@sydney.edu.au

Authors Contributions. P.H. designed the research; G.S. carried out calculations; G.S. and P.H. analyzed data; and G.S. and P.H. wrote the paper.

Competing Interest Statement: Authors declare they have no competing interests.

Keywords: glass solidification, atomic restraint, amorphous order parameter, fragility

Abstract

The persistent problem posed by the glass transition is to develop a general atomic level description of a solidification process that is not associated with any change in the symmetry of the atomic structure. The answer proposed in this paper is to measure a configuration's capacity to restrain the motion of the constituent atoms. Here we show that the instantaneous normal modes can be used to define a measure of atomic restraint that accounts for the difference between fragile and strong liquids and the collective length scale of the supercooled liquid. These results represent a significant simplification of the description of amorphous solidification and provide a powerful systematic treatment of the influence of microscopic factors on the formation of an amorphous solid.

Significance Statement

How do we describe, at a microscopic level, the amorphous solidification of a rapidly cooled liquid into a glass when all that apparently differentiates the structures of the two states is that one is fluid and the other solid? Answering this problem is the key to constructing a conceptual framework for glass formation. In this paper we present a general order parameter for atomic restraint in a liquid and demonstrate that fragility, finite size effects, the influence of pinning and the associated collective length scales, all conventionally defined using dynamic properties, can be characterized as purely structural phenomena. This treatment is quite general, with the potential of treating all solidification processes, ordered and disordered, within a common framework.

Introduction

For any solid to form, crystalline or amorphous, it must achieve a configuration in which each atom is highly restrained. This capacity of a configuration to mechanically restrain the displacements of the constituent particles represents an essential property of solid configurations. For particles interacting via short range repulsions, this restraint at zero temperature can be described by constraint counting [1-4]. A general structural measure for atomic restraint that can apply to any system of interaction particles at any temperature would represent an order parameter capable of describing any solidification and specifically, amorphous solidification. In this paper we shall pursue this line of reasoning. To do so, we must address two questions. The first is the technical issue of defining such an order parameter. This is the subject of the first two Sections of the paper. Once we have a satisfactory order parameter, it follows that we can adopt the general strategy for phase transformations, i.e. we can describe the amorphous solidification in terms of the temperature dependence of that order parameter. In doing so, we shall no longer need slow dynamics as a means of characterizing the transformation. Just to be quite clear, the amorphous solidification that we describe here is not the same as the glass transition. The latter is defined solely in terms of a change in dynamics while the former is defined solely in terms of a change in structure. The causal connection between the two, i.e. the manner in which structure influences dynamics, remains a challenging problem. While we [5] and others [6] have established clear correlations between spatial heterogeneity of vibrational modes of amorphous groundstates and that of intermediate time dynamics, this correlation falls well short of a predictive description of the evolution of an amorphous configuration. The goal of this paper is to explore what progress we can make in describing the formation of glassy solids while avoiding the complexities of the associated kinetics.

If the description of amorphous solidification is not intended to provide an (immediate) explanation of the timescale of relaxation dynamics, what *is* it good for? This is the second (and larger) question we shall address. The answer rests with identifying those features of the phenomenology of the transformation of a liquid into a glass that *can* be recast into questions about the underlying structural change. This recasting should be possible in those instances where the dynamics serves, not as the primary focus, but as a convenient observable signature of some underlying feature of the structure. An example of this situation is the fragility of a liquid. While conventionally associated with the temperature dependence of viscosity, fragility, as first conceived by Angell in 1985 [7], was introduced to describe a feature of the underlying structure of the liquid. In Section 3 of this paper, we shall confirm Angell's original expectation, i.e. that a liquid with a temperature dependent activation energy (a 'fragile' liquid) also exhibits a large temperature dependence in structure while another liquid with temperature -independent

activation energy (a ‘strong’ liquid) exhibits a structure with only a weak dependence on temperature. A second example of dynamics being used to illuminate an underlying structural correlation are kinetic correlation lengths. In Section 5 we shall establish how correlation lengths arise directly as a consequence of the structural change associated with cooling the amorphous material.

Order parameters play a fundamental role in the statistical description of the transformation between two phases. While these transformations are often associated with thermodynamic singularities, an order parameter description is of greater generality and can be applied equally to solidification due to kinetic arrest without any associated singularity or unique transition point. In cases where the phase transformation involves a change in symmetry of the microscopic structure, the choice of order parameter is usually dictated to be a measure of the structure associated with the broken symmetry.

Magnetization in the Ising model or, in the case of the isotropic-nematic transition, the second moment of the distribution of orientation cosines are examples of broken symmetry order parameters. In the case of more complex transformations, there may be multiple options for the order parameter. The freezing of a liquid into a crystal is such a case. In the 1979 density functional theory of Ramakrishnan and Yussouff [8], the order parameters are Fourier amplitudes of the singlet density. In 1984, Tarazona [9] proposed that the singlet density be treated as a sum of Gaussians centered on the crystal lattice sites so that the width of the Gaussian served as the order parameter for crystallization. While useful in the functional theories, these order parameters proved to be of little use in monitoring crystal-like fluctuations in the liquid. To address this problem, Steinhardt et al [10] introduced a bond order parameter based on the amplitudes of spherical harmonics of the local coordination geometry. This order parameter’s evolution has continued with important modifications by Lechner and Dellago [11]. We present this history to establish the point that the choice of an order parameter, while constrained by the twin conditions that i) it quantifies a property defined for individual configurations, and ii) it clearly differentiates the two states involved in the transformation, retains a considerable freedom of choice. Any choice of order parameter is ultimately assessed and improved upon on the basis of its usefulness rather than some *ab initio* proof of worth, a point we ask the reader to keep in mind as we develop the order parameter in this paper.

Topological measures that generalize the bond order parameter of refs. [10,11] have been used to describe amorphous structures. These measures include Voronoi and Delaunay tessellation [12], common neighbor analysis [13] and tetrahedrality [14]. A significant number of these papers are not directly interested in the formation of the amorphous solid but, instead, are looking for the growth of non-crystalline structures that could kinetically obstruct crystal nucleation [15]. The role of local structure on dynamical arrest has been reviewed by Royall and Williams [16]. The effect of the imposed local structure on the

liquid dynamics [17,18] have provided particularly explicit connection between structure and incipient solidity. It remains unclear, however, whether a workable solid order parameter can be extracted from the local topology of a liquid. One difficulty is the huge diversity of local structure in a typical glass. Where crystals rarely exceed 4 distinct local coordination geometries [19], an amorphous solid can have over 100 local topological arrangements [20] that contribute significantly to the structure.

With multiple local structures capable of contributing to restraint, we turn to restraint itself as providing the most generic criteria for quantifying an amorphous configuration. Tarazona's [9] Gaussian expansion of the density, already mentioned, provides perhaps the first explicit measure of solidity in terms of an order parameter based on the degree of atomic restraint. His idea was extended to amorphous solids by Singh et al [21] who retained the Gaussian sum but replaced the crystal lattice with an amorphous structure. The thermodynamic treatment of amorphous solids, initiated in ref. [21], has evolved significantly over the years [22,23]. The associated order parameter is now defined [23] as the average of the overlap Q between two liquid configurations, \vec{r}_α^N and \vec{r}_β^N ,

$$Q[\vec{r}_\alpha^N, \vec{r}_\beta^N] = \frac{1}{N} \sum_{i,j} w(|\vec{r}_{\alpha,i} - \vec{r}_{\beta,j}| / a) \quad (1)$$

where $w(y)$ is a step function, equal to 1 for $y < 1$ and 0 otherwise and a is the resolving length. The average of Q could represent the average restraint about a reference configuration, with $Q \sim 1$ indicating that particles in the reference state are well restrained, at least under the sampling used to calculate the average. The problem is that, with the exception of the crystal structure, most choices of reference state and sampling ensemble result in $\langle Q \rangle = 0$. Franz and Parisi [24] proposed a modified sampling in which they imposed an artificial potential $V(Q)$ defined as the minimal work needed to keep a system at temperature T at a fixed value of Q from a typical equilibrium configuration of the same system. On lowering T , a minimum in V at a $Q^* \neq 0$ appears [25] representing the existence of an underlying metastable state of the unperturbed Hamiltonian, one characterized by a mean restraint Q^* about the reference configuration. While the formalism of ref. [24,25] represents an elegant strategy for the thermodynamic treatment of metastable states, it is not appropriate for the task of mapping a restraint order parameter in an instantaneous configuration.

Results

The Configurational Restraint Parameter

We define the degree of restraint experienced by particles in an instantaneous configuration in terms of the equilibrium amplitude of the individual particle displacements $\langle \Delta r_j^2 \rangle_{eq}$ in a harmonic approximation of the Hamiltonian about that configuration. (Note that we have defined here the meaning of the term ‘restraint’. This definition does not depend on whether our property actually reproduces the dynamical effect of a particle trapped by a persistent cage of its neighbors. We shall return to this distinction later in the paper.) Other measures are possible but this one is efficient to calculate and easily generalizable to any differentiable potential. To generate the harmonic approximation, we shall calculate the instantaneous normal modes (INM’s) and their associated eigenvalues. The INM analysis alone, however, will typically not generate the harmonic potential we are after due to the presence of negative eigenvalues, a problem that we shall address below. These modes, which we shall refer to as ‘unstable’, have been the central focus of much of the literature on the harmonic analysis of liquids due to their possible role in particle dynamics [26,27]. In this paper we employ the INM’s for a quite different purpose. Instead of treating the INM’s as representations of the actual short time dynamics of the liquid, we use them as a tool for identifying resolving the capacity of a configuration to restrain motion and, hence, generate our order parameter. From this perspective, each unstable mode simply represents an absence of information concerning the bounds on the fluctuations of the associated mode amplitude, a lack that we shall address using anharmonic contributions as explained below.

Previously, characterizations of the glass transition have been developed based on an estimation of the local Debye-Waller (DW) factor, $\langle \Delta r_j^2 \rangle_{\tau}$, the mean squared displacement for some fixed short time interval τ . In contrast, $\langle \Delta r_j^2 \rangle_{eq}$, calculated from the harmonic Hamiltonian (described below) is not a dynamic quantity. It is obtained by analysis of a single instantaneous configuration only and therefore should be regarded as a structural measure. As we shall demonstrate, $\langle \Delta r_j^2 \rangle_{\tau} \neq \langle \Delta r_j^2 \rangle_{eq}$ except at very low T . A number of proposals use the local Debye-Waller (DW) factor, not to describe the structure, but to estimate, either directly or implicitly, the temperature dependence of a relaxation time [28-31]. The local DW factor has been used explicitly as an order parameter in some recent studies. Yang et al [32] made use the local DW factor calculated from the dynamical matrix. Ding et al [33] introduced a composite order parameter consisting of the product of the Voronoi volume and the local DW factor. Finally, Tong and Xu [34] quantified the structural heterogeneity of the $T = 0$ glass structures using a measure proportional to $\langle \Delta r_j^2 \rangle_{eq}$, calculated from the normal mode analysis, but only for the $T = 0$ glass structure. While acknowledging the similarities of ref. [32-34] with the present work, we point out two differences that will prove

significant. The first is methodological – our use of $\langle \Delta r_j^2 \rangle_{eq}$ rather than $\langle \Delta r_j^2 \rangle_\tau$ for all temperatures allows us to completely remove dynamics from the definition of the order parameter and, as we shall show, provides a more complete characterization of structure. The second difference is conceptual – where these previous papers have focused almost solely on establishing a correlation between structure and dynamics, we argue here that a restraint order parameter can be more usefully applied to a broader range of phenomenology associated with amorphous solidification.

As we do not make any use of dynamic information, we can sample configurations using Monte Carlo (MC) algorithms. Unless otherwise indicated, all calculations have been carried out using the $A_{80}B_{20}$ Lennard-Jones mixture introduced by Kob and Andersen [35] with 5000 particles in a simulation cell with periodic boundary conditions. Configurations are generated using particle swap MC simulations [36] at constant NVT with a fixed number density of 1.2. From the point at which the average potential energy deviates from linear dependence on T (see Supplementary Material) we determine that the liquid is equilibrated down to $T = 0.36$, below which the configurations we generate are no longer at equilibrium.

In Fig. 1a we plot the temperature dependence of the fraction f_u of unstable modes (i.e. those with negative eigenvalues). We find that the fraction of unstable modes decreases monotonically with decreasing T and vanishes at $T \sim 0$. As shown, our values of f_u are in good agreement with the previous calculations of Donati et al [37]. We calculate $\langle \Delta r_j^2 \rangle_{eq}$ in terms of the amplitudes A_α of the instantaneous normal modes via

$$\langle \Delta r_j^2 \rangle_{eq} = \sum_{\alpha} \langle A_{\alpha}^2 \rangle_{eq} (\vec{v}_{\alpha}^j)^2 \quad (2)$$

where \vec{v}_{α}^j is the components of the α eigenmode arising from particle j . If the eigenvalue $\lambda_{\alpha} > 0$, the average $\langle A_{\alpha}^2 \rangle_{eq}$ can be evaluated analytically as

$$\langle A_{\alpha}^2 \rangle_{eq} = k_B T / \lambda_{\alpha} \quad (3)$$

For those unstable modes with $\lambda_{\alpha} \leq 0$, Eq. 3 cannot be used. Instead, we numerically integrate

$$\langle A_{\alpha}^2 \rangle_{eq} = \frac{\int A_{\alpha}^2 e^{-\beta U(A_{\alpha})} dA_{\alpha}}{\int e^{-\beta U(A_{\alpha})} dA_{\alpha}} \quad (4)$$

where $U(A_\alpha)$ is the true potential energy calculated as a function of the variation of the amplitude A_α , holding all other mode amplitudes at zero and $\beta = (k_B T)^{-1}$. An example of the potential profile $U(A_\alpha)$ for an unstable mode is presented in Fig. 1b where we note that, with the inclusion of the anharmonic contributions, $U(A_\alpha)$ provides a well-defined bound on the mode amplitude fluctuations, even when the harmonic term alone does not.

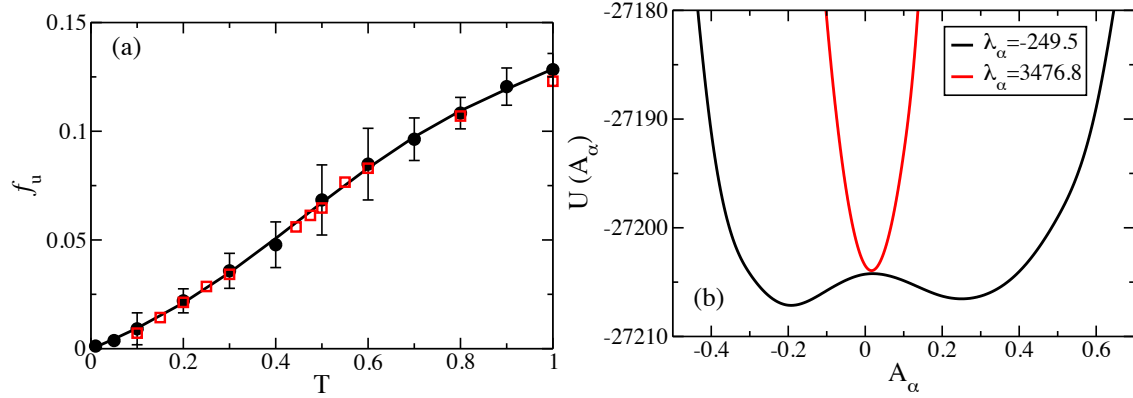


Figure 1. a) The fraction f_u of unstable modes as a function of T for the KA liquid. The black circles are from the present paper while the red squares are data from ref. [37]. The vertical lines represent one standard deviation above and below the mean. b) Examples of the potential energy surface $U(A)$ associated with the variation in amplitude A_α of an unstable (black line) and stable (red line) mode.

It is useful for an order parameter to be restricted in value to the interval $(0,1)$. We define, therefore, a general order parameter μ_j for the restraint of atom j as

$$\mu_j = \exp\left(-\frac{q^2 \langle \Delta r_j^2 \rangle}{6}\right) \quad (5)$$

where q is the magnitude of the wavevector of the first peak in the structure factor $S(q)$, a value that varies little with temperature under the constant volume constraint (see

Supplementary Material). In Fig. 2a we plot the average restraint $\langle \mu \rangle = \frac{1}{N} \sum_i \mu_i$ as a

function of T . The increase in $\langle \mu \rangle$ on cooling provides an explicit measure of the progress of amorphous solidification on cooling.

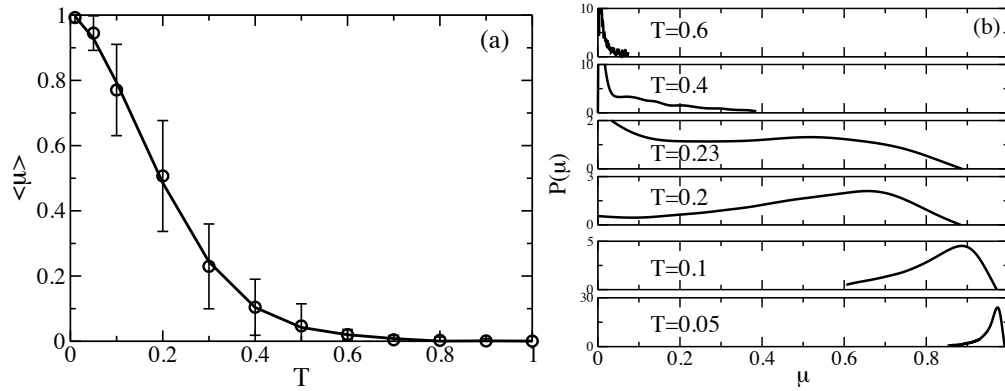


Figure 2. a) The plot of the average restraint $\langle \mu \rangle$ as a function of T for the KA liquid. The vertical lines represent one standard deviation above and below the mean. b) The distribution of μ for a range of temperatures, as indicated. For reference, the freezing point of the KA mixture is $T_m = 1.02$ [38].

We find that the average restraint exhibits a nonlinear increase with decreasing T . This change is associated with the appearance of a broad binodal distribution in μ with a maximum of in the variance at $T \sim 0.23$ with peaks at 0 and ~ 0.6 as shown in Fig. 2b. It follows directly that the configurational restraint exhibits a maximum in heterogeneity at this transformation temperature. We emphasize that the temperature dependent changes in the order parameter μ describe a purely structural change in the instantaneous configurations during the transition from liquid to amorphous solid.

On the Difference in Configurational Restraint between Strong and Fragile Liquids.

As discussed in the Introduction, having defined a sensible order parameter we still have to establish just what phenomena can be usefully treated from this structural perspective. Our first candidate will be the striking difference between the glass transitions of oxide glass formers such as SiO_2 and the transition in liquids governed by largely isotropic interactions (i.e. molecular and metallic liquids). A measure of this difference is the temperature dependence of the effective activation energy for relaxation. In the case of the network-forming liquids ('strong' in Angell's classification) the activation energy is independent of T while in molecular liquids ('fragile'), the activation energy increases nonlinearly with decreasing temperature [7]. Can the description of these two transitions based on the order parameter μ capture an underlying structural difference?

Molten silica has been modelled with molecular dynamics using the SHIK-1 potential [39] which includes long range Coulomb interaction. The use of the PPPM [40], a Fourier-based Ewald summation method, to calculate the Coulomb contribution to the

potential energy complicates the analytic calculation of the Hessian. We have used numerical differentiation to calculate the second derivations of the energy (details provided in the Supplementary Information). The fraction of imaginary modes in the model silica was found to be small, < 0.08 over the T range studied. The treatment of these modes and the subsequent calculation of the restraint $\{\mu_i\}$ was carried out as for the Lennard-Jones system. To usefully compare our two model liquids, we have plotted the results in Fig. 3 in terms of a reduced temperature T/T_m , using the following values of the melting points: for SHIK-1 silica $T_m = 2400\text{K}$ [41] and for the KA alloy, $T_m = 1.02$ [38].

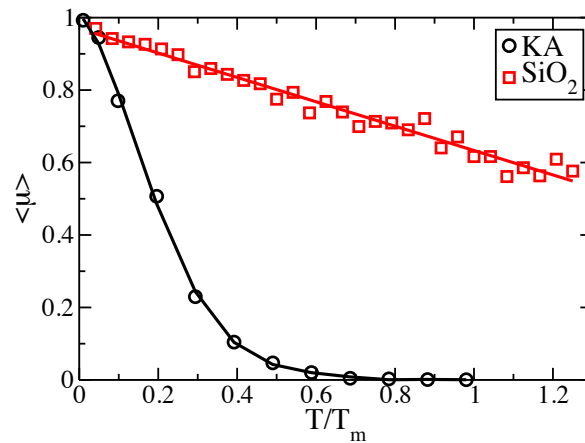


Figure 3. Plot of $\langle \mu \rangle$ vs T/T_m for the KA mixture and for silica. The temperature has been scaled by the respective melting points T_m (provided in the text) solely to allow comparison between the data from the different liquids.

The difference in the temperature dependence of the configurational restraint between silica and the atomic mixture is striking. Where the atomic mixture exhibits an abrupt increase in restraint at a temperature well below the melting point, silica maintains a high degree of restraint all the way up to the boiling point. This result, suggestive as it is, does not explicitly allow us to account for the difference in activation energies. This challenge we leave to future work. It does, however, allow us to identify a *structural* fragility that appears to align with the conventional *dynamic* fragility. Angell has proposed an overarching account of the glass transition based on the existence of just such a structural fragility in the form of an underlying continuous order-disorder transition [42]. In this picture the distinction between fragile and strong liquids is determined by whether this transition occurs below or well above T_m , respectively. There are obvious parallels between our results and Angell's proposal. The differences are that a) we present an

explicit measure of the structural change associated with the underlying transformation and b) our transformation is not a cooperative thermodynamic order-disorder transition, a result we shall establish in Section 5.

What we demonstrate here is that these liquids, the atomic alloy and silica, are differentiated by their structural fragility. The structure of a strong liquid, even at equilibrium, lies close enough to that of the amorphous solid that there is little room for further development on cooling, the very development that characterizes the fragile liquid. One consequence of this result is the observation that, in the case of silica, the liquid is, structurally, indistinguishable from that of a hot solid. The inability of our order parameter to identify the liquid state in this case is, perhaps, not surprising. The viscosity of silica at its melting point is $\sim 10^5$ times the corresponding values for most fragile liquids. In the context of current timescales accessible to MD simulation, the silica melt does indeed resemble a solid at T_m .

Configurational Restraint and the Self Intermediate Scattering Function

In supercooled liquids, the self-intermediate scattering function $F_s(q,t)$,

$$F_s(q,t) = \frac{1}{N} \left\langle \sum_j^N \exp(i\vec{q} \cdot \Delta\vec{r}_j(t)) \right\rangle \quad (6)$$

taken at a value of the wavevector q corresponding to the first peak of the structure factor $S(q)$, is referred to as the structural relaxation function. The decay of this function in the supercooled liquid, as shown in Fig. 4a, proceeds via a two step process; a fast relaxation to a plateau value, h , which is subsequently relaxed by slower mechanism, the α process, with a strong temperature dependence. Previously, in the plateau height h has been identified as a ‘non-ergodicity’ parameter and linked to an order parameter developed for spin glasses [43]. In the limit of a harmonic solid, it can be shown that $h = \langle \mu_i \rangle$ which raises the question, whether $\langle \mu \rangle$ is essentially equivalent to the plateau value h of $F_s(q,t)$ for all T ?

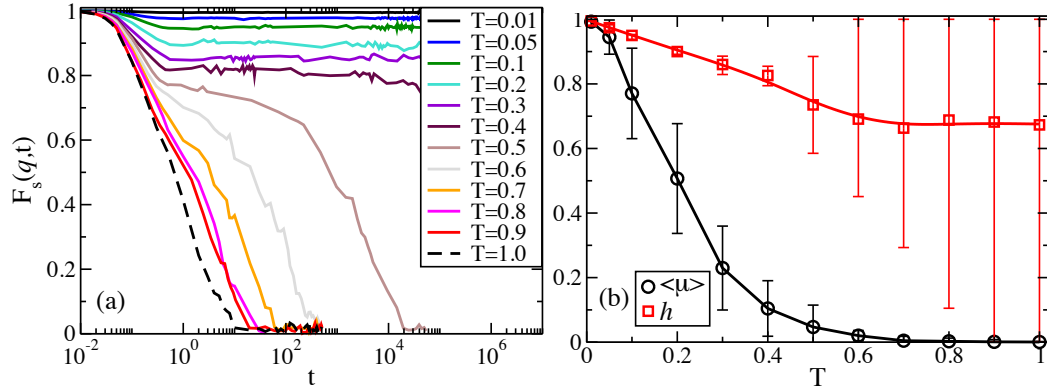


Figure 4. a) Plots of the self intermediate scattering function $F_s(q,t)$ vs log time for range of temperatures for the KA liquid. b) Plot of the plateau height h of $F_s(q,t)$ and μ as a function of T . Note the large uncertainty in h at high T due to the lack of a well-defined plateau. Details of the calculation of h and the associated uncertainty are provided in the Supplementary Materials.

In Fig. 4b we establish that $\langle \mu \rangle \neq h$, with the restraint $\langle \mu \rangle$ exhibiting a much stronger dependence on temperature than h , dropping to zero over a temperature range for which the plateau exhibits only a weak variation. We also note that h becomes ill-defined for $T > 0.6$ due to the disappearance of the plateau. The fact that $\langle \mu \rangle$ is smaller than h is perhaps surprising since the former corresponds to an average over a highly restricted set of fluctuations while the latter has no imposed constraints. The explanation is that the large amplitude fluctuations responsible for the small values of μ are not accessible to the dynamics on the lifetime of given instantaneous configuration. The short time dynamics cannot ‘see’ the softest modes supported by the individual configurations due to this motional ‘stiffening’. This observation underlines the point, already made, that $\langle \mu \rangle$ is not presented as a predictor of short time dynamics but as an order parameter whose essential function is to differentiate fluid and solid amorphous structures.

Amorphous Solidification under Imposed Restraint: Pinning and Finite Size Effects

As we have defined it, the structural transformation from liquid to amorphous solid depends, not on the appearance of special topologies but, rather, on the presence of *any* structure capable of exerting local restraint. We can adjust this restraining influence, without change to the configurational geometry, by pinning random particles. Let

$M = (1-c)N$ be the number of unpinned particles where c is the fraction of pinned particles. Following ref. 44, the impact of pinning on the instantaneous normal modes is calculated by diagonalizing the $3M \times 3M$ Hessian matrix consisting of only derivatives of

coordinates of the unpinned particles. Note that the pinning is only applied when calculating the normal modes - not during the MC simulation used to generate the configurations.

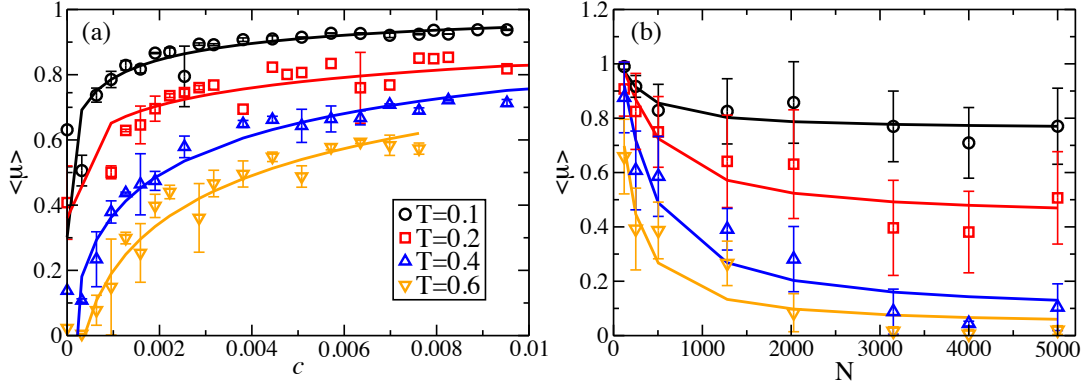


Figure 5. The dependence of the average restraint $\langle \mu \rangle$ as a function of a) the fraction of c pinned particles and b) the system size N , for a number of temperatures for the KA liquid as indicated. The solid curves correspond to the curve in Eq.6 and 7, respectively, with fitted lengths ξ and ζ listed in Table 1.

As shown in Fig. 5a, we find that the mean restraint increases quickly with the addition of a low density of pinned particles only to show signs of saturation as c is increased. This increase in $\langle \mu \rangle$ steadily shifts our fragile alloy towards the values of restraint that characterize silica in Fig. 3. This structural shift from fragility to strong due to pinning is consistent with the analogous shift in kinetic behavior reported in ref. [45]. The concentration of pinned particles required to shift $\langle \mu \rangle$ by some amount can be expressed in terms of a length scale ξ over which a pinned particle ‘influences’ its surroundings. We find the following expression,

$$\langle \mu(c) \rangle = 1 - (1 - \langle \mu(0) \rangle) \exp(-\xi c^{1/3}) \quad (7)$$

provides a satisfactory description of our data and include the fitted values of the fitted length scale ξ at various values of T in Table 1. The modest increase in the length ξ on cooling is similar to that reported in ref. [45]. It is useful to emphasize that this length is, by construction, purely mechanical in nature, and related to the density of pinned particles necessary to pin sufficient unstable modes to achieve the desired increase in restraint. This length does not correspond to a correlation length associated with thermal

fluctuations because we do not include the pinning during the MC calculation, i.e. the pinning here is essentially just a modification of the normal analysis so cannot effect the sampling of configurations.

	T=0.1	T=0.2	T=0.4	T=0.6
ξ (pinning) Eq. 7	7.0	5.5	4.7	4
ζ (N dep.) Eq. 8	6.55	6.4	6.3	5.2

Table 1. The length scales ξ and ζ obtained from pinning (Eq. 7) and finite size effects (Eq. 8), respectively, for the KA liquid.

A related question is the influence of system size on the amorphous solidification described by the temperature dependence of restraint. As particle restraint is a consequence of many-bodied correlations, it should exhibit some sort of characteristic length. In Fig. 5a we plot $\langle \mu \rangle$ vs T for different values of N. For $N < 500$ we find that the T dependence of the $\langle \mu \rangle$ broadens with decreasing system size and, as for pinning, the degree of restraint increases, indicating a fragile-to-strong transition with decreasing systems size. In Fig. 5b we plot $\langle \mu \rangle$ as a function of N and find the dependence of $\langle \mu \rangle$ on N is described by,

$$\langle \mu(N) \rangle = 1 - (1 - \langle \mu(\infty) \rangle) \exp(-\xi^3 / N) \quad (8)$$

The associated length ζ , obtained by fitting, is similar in magnitude and T dependence to that obtained from pinning (see Table 1). Karmakar, Procaccia and coworkers [46,47] reported a system size dependence of the structural relaxation time of the KA mixture with a similar scaling to that in Eq. 6 and with a similar T dependent increase as that reported in Table 1. In ref. [47], this scaling length was found to match a length obtained directly from a normal mode analysis. The idea [47] is that minimum eigenvalue of the inherent structure exhibits a crossover from a plastic mode to a Debye vibration as N increases, with the crossover size providing the length. The connection between this length and the one we extract here from the INM's is an interesting question. The crossover length of ref. [47] is found [48] to be the same as that obtained by the 'point-to-set' method [49], a variant of pinning, a result consistent with the similarity we find between the pinning and finite size scaling lengths in Table 1.

The modest increase in the length scales as provided in Table 1, along with absence of power law scaling, indicates that the structural transformation we describe in Fig. 2 is not associated with a thermodynamic singularity [50]. It has been proposed [51] that the transition to the amorphous solid arises as a result of the growing correlation length. Our results suggest a different interpretation, one in which the length scales arise as a consequence of the increasing restraint, not as the cause, and that these lengths reflect the mechanical character of the individual configurations, specifically the characteristic length scales associated with the unstable modes of the INM's, and not the result of some correlation between thermally sampled configurations.

Conclusion and Discussion

In this paper we have demonstrated that there exists a quantifiable change in structure that provides an explicit characterization of the transformation, on cooling, of a liquid into an amorphous solid, one that can account, in purely structural terms, for the differences in vitrification of fragile and strong liquids, and the impact of imposed constraints such as pinning and finite size. Previously [52] we have established that a related measure of restraint can account for the enhanced kinetics at a glass surface.

Where the conventional account of the glass transition uses the increase of the relaxation times to measure the continuous shift of the supercooled state *away* from fluidity, the order parameter we introduce describes the solidification by measuring the continuous structural approach of the state *towards* the amorphous solid. This solid-centric approach allows us to describe amorphous solidification in a manner that is similar to the approach used to describe other solidification processes. The benefits, we argue, are the technical simplification and greater versatility over descriptions based on long time dynamics, the clearer conceptual path between structure and the details of the interactions between particles and, finally, the value of aligning the description of amorphous solidification within the general theoretical framework of materials science.

Beyond the technical innovation of the restraint order parameter, we have sought to demonstrate that the associated structural phenomenology – fragility, size dependence and the pinning length scale – closely parallels the rich phenomenology previously reported in terms of the dynamics. The structural phenomenology allows for straight forward explanations. Silica is distinguished from the alloy by the large magnitude and weak temperature of the density of restraint. The length scale associated with the change in structure due to increasing the concentration of pinning particles or decreasing the size of the system results because both of these constraints depress the number of unstable and low frequency modes, hence stiffening the liquid. This purely mechanical account of a temperature dependent length scale avoids speculations about avoided transition, the growth of clusters of favored coordination or the transmission of kinetic facilitation.

While these phenomena may well be present in the supercooled liquid, they cannot be attributed as the cause of the lengths reported here.

What of dynamics? The conventional representation of amorphous solidification is based on equating solidity with a shear viscosity in excess of some threshold value, a phenomenological view that regards slow dynamics as the primary *cause* of amorphous solidification. We have argued here that solidity can be usefully treated as a structural property, implying that dynamics arises as a *consequence* of the structural transition on cooling. While there is no shortage of empirical correlations supporting this link [27-30], establishing the theoretical connection between structure and dynamics remains a hard problem, in large part because dynamics requires more information (e.g. extent of reorganization events, reversibility, etc.) than a single configuration provides. We note that the local harmonic basin we construct out of the instantaneous normal modes can provide considerably more information than that to be found in the restraint order parameter. We leave to future work the possibility of establishing a connection between structure and dynamics by exploring the nature of structural fluctuations within the harmonic Hamiltonian.

In defining an order parameter based on restraint we have a measure of considerable generality. Amorphous solidification represents a rich field of phenomena with important practical applications and unresolved fundamental questions. The nature of amorphous surfaces, the impact of atomic association ('micro alloying'), the role of molecular shape and internal flexibility, the consequences of applied strain, gelation and the precipitation of framework compounds – all of these questions can be addressed as structural problems based on the distribution of atomic restraint through straightforward applications of the methodology introduced in this paper.

Data Availability Statement. All the data supporting the findings of this study are available within this paper and the Supplementary Information. Additional information is available from the corresponding author upon reasonable request.

Acknowledgements

The authors gratefully acknowledge the assistance of Linwei Li in the generation of data for the silica system and the support from the Australian Research Council Discovery Project grant DP180104038 (PH).

References

1. C. S. O'Hern, L. E. Silbert, A. J. Liu and S. R. Nagel, Jamming at zero temperature and zero applied stress: The epitome of disorder. *Phys. Rev. E* **68**, 011306 (2003).

2. M. Wyart, On the rigidity of amorphous solids. *Ann. Rev. Fr.* **30**, 1-96 (2005).
3. M. van Hecke, Jamming of soft particles: geometry, mechanics, scaling and isostaticity. *J. Phys. Cond. Matter* **22**, 033101 (2010).
4. A. J. Liu and S. R. Nagel, The jamming transition and the marginally jammed solid. *Ann. Rev. Cond. Matter Phys.* **1**, 347-369 (2010).
5. A. Widmer-Cooper, H. Perry, P. Harrowell and D. R. Reichman, Irreversible reorganization in a supercooled liquid originates from localized soft modes. *Nature Phys.* **4**, 711-715 (2008).
6. J. Ding, S. Patinet, M. Falk, Y. Cheng and E. Ma, Soft spots and their structural signature in a metallic glass. *Proc. Nat. Acad. Sci USA* **111**, 14052-14056 (2014).
7. C. A. Angell, Spectroscopy simulation and scattering, and the medium range order problem in glass. *J. Non-Cryst. Sol.* **73**, 1-17 (1985).
8. T. V. Ramakrishnan and M Yussouff, First principles order-parameter theory of freezing. *Phys. Rev. B* **19**, 2775 (1979).
9. P. Tarazona, A density functional theory of melting. *Mol. Phys.* **52**, 81 (1984).
10. P. Steinhardt, D. Nelson, and M. Ronchetti, Bond orientational order in liquids and glasses. *Phys. Rev. B* **28**, 784 (1983).
11. W. Lechner and C. Dellago, Accurate determination of crystal structures based on averaged local bond order parameters. *J. Chem. Phys.* **129**, 114707 (2008).
12. Y. Hiwatari, T. Saito and A. Ueda, Structural characterization of soft-core and hard-core glasses by Delaunay tessellation. *J. Chem. Phys.* **81**, 6044 (1984).
13. J. D. Honeycutt and H. C. Andersen, Molecular dynamics study of melting and freezing of small Lennard-Jones clusters. *J. Phys. Chem.* **91**, 4950-4963 (1987).
14. S. Marin-Aguilar, H. H. Wensink, G. Foffi and F. Smallenburg, Tetrahedrality dictates dynamics in hard sphere mixtures. *Phys. Rev. Lett.* **124**, 208005 (2020).
15. K. J. Laws, D. B. Miracle and M. Ferry, A predictive structural model for bulk metallic glasses. *Nature Comm.* **6**, 8123 (2015).
16. C. P. Royall and S. R Williams, The role of local structure in dynamical arrest. *Phys. Rep.* **560**, 1-75 (2015).
17. C. De Michele, S. Gabrielli, P. Tartaglia, F. Sciortino, Dynamics in the presence of attractive patchy interactions. *J. Phys. Chem. B* **110**, 8064–8079 (2006).

18. S. Marin-Aguilar, H. H. Wensink, G. Foffi and F. Smallenburg, Slowing down supercooled liquids by manipulating their local structure. *Soft Matter* **15**, 9886-9893 (2019).
19. J. L. C. Daams and P. Villars, Atomic environment classification of the tetragonal ‘intermetallic’ structure types, *J. Alloys Comput.* **252**, 110 (1997).
20. D. Wei, J. Yang, M.-Q. Jiang, L.-H. Dai, Y.-J. Wang, Dyre, I. Douglass and P. Harrowell, Assessing the utility of structure in amorphous materials. *J. Chem. Phys.* **150**, 114502 (2019).
21. Y. Singh, J. P. Stoessel and P. G. Wolynes, Hard-sphere glass and the density functional theory of aperiodic crystals. *Phys. Rev. Lett.* **54**, 1059 (1985).
22. V. Lubchenko and P. G. Wolynes, Theory of structural glasses and supercooled liquids. *Ann. Rev. Phys. Chem.* **58**, 235-266 (2007).
23. G. Parisi and F. Zamponi, Mean-field theory of hard sphere glasses and jamming. *Rev. Mod. Phys.* **82**, 789-845 (2010).
24. S. Franz and G. Parisi, Recipes for metastable states in spin glasses. *J. Phys. I* **5**, 1401-1415 (1995)
25. B. Guiselin, G. Tarjus and L. Berthier, On the overlap between configurations in glassy liquids. *J. Chem. Phys.* **153**, 224502 (2020).
26. R. M. Stratton, The instantaneous normal modes of liquids. *Acc. Chem. Res.* **28**, 201-207 (1995).
27. B. Maden and T. Keyes, Unstable modes in liquids density of states, potential energy, and heat capacity. *J. Chem. Phys.* **98**, 3342 (1993).
28. J. C. Dyre, T. Christensen and N. B. Olsen, Elastic models for the non-Arrhenius viscosity of glass-forming liquids. *J. Non-Cryst. Sol.* **352**, 4635-4642 (2006).
29. L. Larini, A. Ottochian, C. De Michele and D. Leporini, Universal scaling between structural relaxation and vibrational dynamics in glass-forming liquid and polymers. *Nature Phys.* **4**, 42-45 (2008).
30. D. S. Simmons, M. T. Cicerone, Q. Zhong, M. Tyagi and J. F. Douglas, Generalized localization model of relaxation in glass-forming liquids. *Soft Matter* **8**, 11455(2012).
31. U. Buchenau, R. Zorn and M A. Ramos, Probing cooperative liquid dynamics with the mean squared displacement. *Phys. Rev. E* **90**, 042312 (2014).

32. X. Yang, H. Tong, W.-H. Wang and K. Chen, Emergence and percolation of rigid domains during the colloid glass transition. *Phys. Rev. E* **99**, 062610 (2019).
33. J. Ding, Y.-Q. Cheng, H. Sheng, M. Asta, R. O. Ritchie and E. Ma, Universal structural parameter to quantitatively predict metallic glass properties. *Nature Com.* **7**, 13733 (2016).
34. H. Tong and N. Xu, Order parameter for structural heterogeneity in disordered solids. *Phys. Rev. E* **90**, 010401(R) (2014).
35. W. Kob and H. C. Andersen, Testing mode-coupling theory for a supercooled binary Lennard-Jones mixture – The van Hove correlation function. *Phys. Rev.* **51**, 4626-4641 (1995).
36. T. S. Grigera and G. Parisi, Fast Monte Carlo algorithm for supercooled soft spheres. *Phys. Rev. E* **63**, 045102 (2001).
37. C. Donati, F. Sciortino and P. Tartaglia, Role of unstable directions in the equilibrium and ageing dynamics of supercooled liquids. *Phys. Rev. Lett.* **85**, 1464 (2000).
38. U. R. Pedersen, T. B. Schröder and J. C. Dyre, Phase diagram of Kob-Andersen-type binary Lennard-Jones mixtures. *Phys. Rev. Lett.* **120**, 165501 (2018).
39. S. Sundararaman, L. Huang, S. Ispas, W. Kob, New optimization scheme to obtain interaction potentials for oxide glasses. *J. Chem. Phys.* **148**, 194504 (2018).
40. Y. Zhang, L. Huang and Y. Shi, Molecular dynamics study on the viscosity of glass-forming systems near and below the glass transition temperature. *J. Am. Ceram. Soc.*, **104**, 6227-6241 (2021).
41. A. Takada, P. Richet, C. R. A. Catlow and G. D. Price, Molecular dynamics simulations of vitreous silica structures. *J. Non-Cryst. Solids* **345-346**, 224-229 (2004).
42. C.A. Angell, Glass-formers and viscous liquid slowdown since David Turnbull: Enduring puzzles and new twists. *MRS Bulletin*, **33**, 544-555 (2008).
43. W. Gotze and L. Sjogren, Relaxation processes in supercooled liquids. *Rep. Prog. Phys.* **55**, 241 (1992).
44. L. Angelani, M. Paoluzzi, G. Parisi and G. Ruocco, Probing the non-Debye low-frequency excitations in glass through random pinning. *Proc. Nat. Acad. Sci.* **115**, 8700-8704 (2018).

45. S. Chakrabarty, S. Karmakar and C. Dasgupta, Dynamics of glass forming liquids with randomly pinned particles. *Sci. Rep.* **5**, 12577 (2015).
46. R. Gutiérrez, S. Karmakar, Y. G. Pollack and I. Procaccia, The static lengthscale characterizing the glass transition at lower temperatures. *EPL* **111**, 56009 (2015).
47. S. Karmakar, E. Lerner and I. Procaccia, Direct estimate of the static length-scale accompanying the glass transition. *Physica A* **391**, 1001-1008 (2012).
48. G. Biroli, A. Karmakar and I. Procaccia, Comparison of static length scales characterizing the glass transition. *Phys. Rev. Lett.* **111**, 165701 (2013).
49. J.-P. Bouchaud and G. Biroli, On the Adam-Gibbs-Kirkpatrick-Thirumalai-Wolynes scenario for the viscosity increase in glasses. *J. Chem. Phys.* **121**, 7347 (2004).
50. K. Binder, Finite size effects on phase transitions. *Ferroelectrics* **73**, 43-67 (1987).
51. S. Karmakar, C. Dasgupta and S. Sastry, Growing length scales and their relation to timescales in glass-forming liquids. *Ann. Rev. Cond. Matter Phys.* **5**, 255-284 (2014).
52. G. Sun, S. Saw, I. Douglass and P. Harrowell, Structural origin of enhanced dynamics at the surface of a glassy alloy. *Phys. Rev. Lett.* **119**, 245501 (2017).

A General Structural Order Parameter for the Amorphous Solidification of a Supercooled Liquid

Gang Sun, Peter Harrowell*

* Correspondence to: peter.harrowell@sydney.edu.au

This file includes:

1. Simulations and Normal Mode Analysis of the KA Mixture
2. Simulations of the SHK Silica and Calculation of the Hessian
3. Effect of Pinning and System Size on the Distribution of Normal Modes
4. Calculation of Plateau Height h and its Associated Error
5. The variance of structural restraint degree on cooling of the KA mixture

1. Simulations and Normal Mode Analysis of the KA Mixture

The Monte Carlo simulations of the $A_{80}B_{20}$ Lennard-Jones mixture use the potential introduced by Kob and Andersen [1] with 5000 particles in a simulation cell with periodic boundary conditions. Well relaxed configurations are generated using particle swap Monte Carlo (MC) simulations at constant NVT with a fixed number density of 1.2.

To simulate the systems, we have used a Monte Carlo algorithm from the DLMONTE 2.0 version suite of software. The random walk in the MC simulations is constructed using a Metropolis scheme that iterates the following three steps:

1. Select a particle i at random and calculate its energy $U(\mathbf{r}_1)$.
2. Displace the particle randomly to a *trial* position and calculate its new energy $U(\mathbf{r}_2)$.
3. Accept or reject the particle displacement according to the Metropolis acceptance rule:

$$P_{\text{acc}}(\mathbf{r}_1 \rightarrow \mathbf{r}_2) = \min(1, \exp\{-\beta[U(\mathbf{r}_2) - U(\mathbf{r}_1)]\})$$

Swap moves are also applied in this work, with the exchange frequency $n=50$ time steps. The details are as follows:

4. Choose a random particle j of a different type.
5. Swap particle positions $\mathbf{r}_j \leftrightarrow \mathbf{r}_i$. Shift both particles as in the standard move
6. Accept or reject new configuration according to the Metropolis criterion
7. Repeat for all particles.

The calculation of the variance of the amplitude A_k of mode k for cases where the eigenvalue $\lambda_k < 0$ were carried out as follows.

A 1D energy curve can be plotted based on the variation of the potential energy U with respect to the selected amplitude A_k while setting all other mode amplitudes to zero. The results for two such curves are shown in Fig. S1, one with $\lambda_k < 0$ and one with $\lambda_k > 0$. In the case of the $\lambda_k < 0$ mode we see the region of negative curvature. While the value of $\langle A_k^2 \rangle$ can be calculated analytically for the $\lambda_k > 0$ case, as indicated by Eq. 3 in the paper, $\langle A_k^2 \rangle$ must be calculated numerically when $\lambda_k < 0$. As can be seen from Fig. S1, this variance is well defined due to the positive contributions of higher order terms in A_k . The numerical integration indicated in Eq. 4 is carried out over the range of A_k for which $\Delta E \leq 10k_B T$ as indicated in Fig. S1. Increasing this threshold produces no change in the calculated value. $10k_B T$ is chosen as energy threshold.

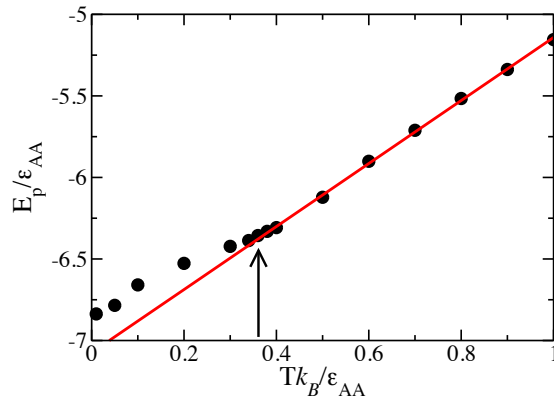


Figure S1. The potential energy of KA mixtures relaxed at various temperature. The arrow indicates the temperature ($=0.36$) where the average potential energy deviates from linear dependence on T .

In Fig. S2 we plot the temperature dependence of the fraction of modes with negative eigenvalues and the distributions of average square $\langle A_\alpha^2 \rangle$'s from the stable and unstable modes. We find that the fraction of unstable modes decreases monotonically with decreasing T and vanishes at $T \sim 0$. As shown in Fig. S2, the amplitudes associated with the unstable modes, evaluated using Eq. 4, are very much larger than those of the stable modes and so contribute significantly to the magnitude of $\langle \Delta r_j^2 \rangle$.

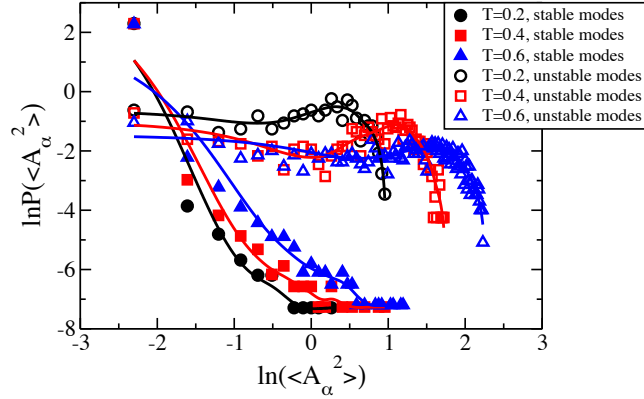


Figure S2. The log-log plot of the distribution of mode amplitudes $\langle A_\alpha^2 \rangle$'s from the stable and unstable modes at $T = 0.6, 0.4$ and 0.2 . The curves are fits included as a visual guide.

2. Simulations of the SHK Silica and Calculation of the Hessian

We perform the molecular dynamics (MD) simulations of silica by using SHIK-1 potentials [2] which have high geometric accuracy. This potential includes long range Coulomb interactions requiring an Ewald sum. The silica systems contain 576 atoms. All the samples are prepared using the melt-quench method. At first, we generate an Alpha-quartz model at 300 K, then we relaxed the quartz at 300K, zero pressure condition for 0.1 ns to release the pressure. After the quartz was relaxed, we heated the quartz to 4000 K at a constant rate over 0.5 ns, then equilibrated the melted sample at a density of 2.2 g/cm^3 for another 0.5 ns in the NVT ensemble. The sample was then quenched to 300 K in the NPT ensemble at a rate of 1 K/ps with zero pressure. After quenching, it was then annealed at 300 K for another 1 ns.

Hessian matrix elements are usually defined as,

$$H_{i\mu,j\nu} = \frac{1}{\sqrt{m_i m_j}} \frac{\partial^2 U}{\partial r_{i,\alpha} \partial r_{j,\beta}} (i, j = 1, \dots, N, \mu, \nu = x, y, z) \quad (\text{S1})$$

Where U is the total potential energy of the system. Since long range interactions are involved in the simulation of silica, analytical expressions for the Hessian matrix elements are complicated. Therefore, we generated the Hessian matrix moving the individual particles from their starting configuration R to $R + \delta r_{j,v}$, in order to counterbalance, a double move of R to $R - \delta r_{j,v}$, is employed. The displacement of 0.0016 \AA has been chosen as it is small enough to avoid any disruption to the structure and gives reasonably accurate result.

$$\sqrt{m_i m_j} H_{i\mu, j\nu} = \nabla_{i,\mu} \nabla_{j,\nu} U = \frac{\psi_{i,\mu}(R + \delta r_{j,v}) - \psi_{i,\mu}(R - \delta r_{j,v})}{2\delta r_{j,v}} \quad (\text{S2})$$

where U is the potential energy and $\psi_{i,\mu}$ is the force of particle i along μ direction.

On diagonalizing the Hessian we find a fraction f of modes with negative eigenvalues that decreases monotonically with temperature and appears to vanish at $T = 0$ as shown in Fig. S3.

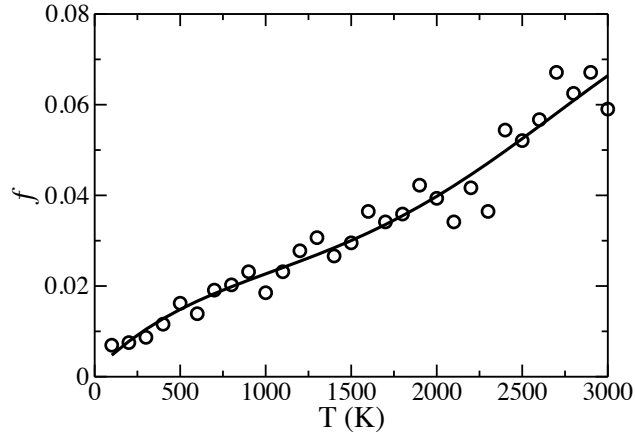


Figure S3. The fraction of unstable modes of silica as function of T.

3. Effect of Pinning and System Size on the Distribution of Normal Modes

The impact of pinning concentration and system size on the restraint order parameter arise from the impact of these parameters on the density of states in the harmonic analysis. This can be seen in Fig. S4 which shows an increase in small amplitude modes and a decrease in small eigenvalue λ modes when we either increase c , the pinning concentration, or decrease N , the system size.

We randomly select the particle ID number in simulation box from 1 to N , by using random number generator. No steps were taken to avoid Poisson clustering of pinning sites.

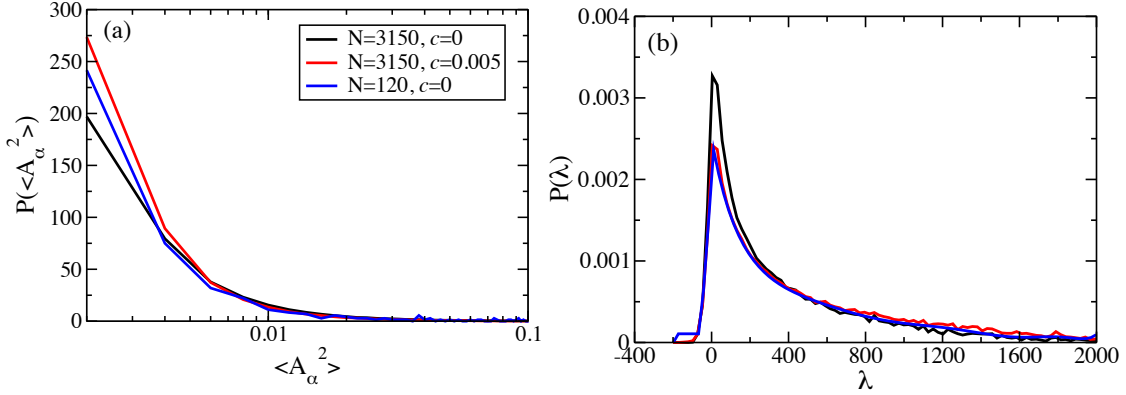


Figure S4. (a) The distribution of the square amplitudes for each mode at $T=0.6$. (b) The distribution of eigenvalues of Hessian Matrix for instantaneous structure from $T=0.6$. Here we include three different systems with system particle number $N=120$ and 3150 , and pinning particle concentration $c=0$ and 0.05 .

4. Calculation of Plateau Height h and its Associated Error

For supercooled liquids, the self intermediate scattering function $F_s(q,t)$, is taken at the a value of the wavevector $q=q_1$, which corresponds to the first peak of the structure factor $S(q)$. The structure factor as function of wavevector is shown in Fig.S5.

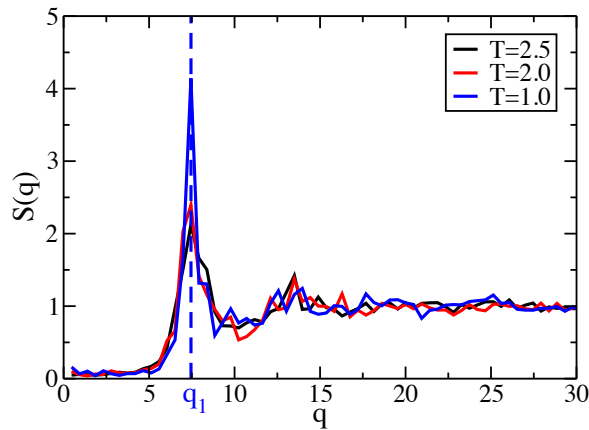


Figure S5. The structure factor $S(q)$ as function of wavevector q for $T=2.5$, 2.0 and 1.0 . The first peak position q is 7.45 .

For liquids, the relaxation occurs in two steps, observed from the self intermediate scattering function $F_s(q_1,t)$ [see Fig.S6]. The two step decays correspond to α relaxation

(slow) and β relaxation (fast). Hence, it is reasonable to fit $F_s(q,t)$ of liquids by a sum of two functions,

$$F_s(q_1, t) = (1 - h) \exp \left[- \left(\frac{t}{\tau_\beta} \right)^2 \right] + h \exp \left[- \left(\frac{t}{\tau_\alpha} \right) \right] \quad (\text{S3})$$

where h is the plateau height of relaxation function F_s . The quality of the fits is demonstrated in two examples plotted in Fig. S6.

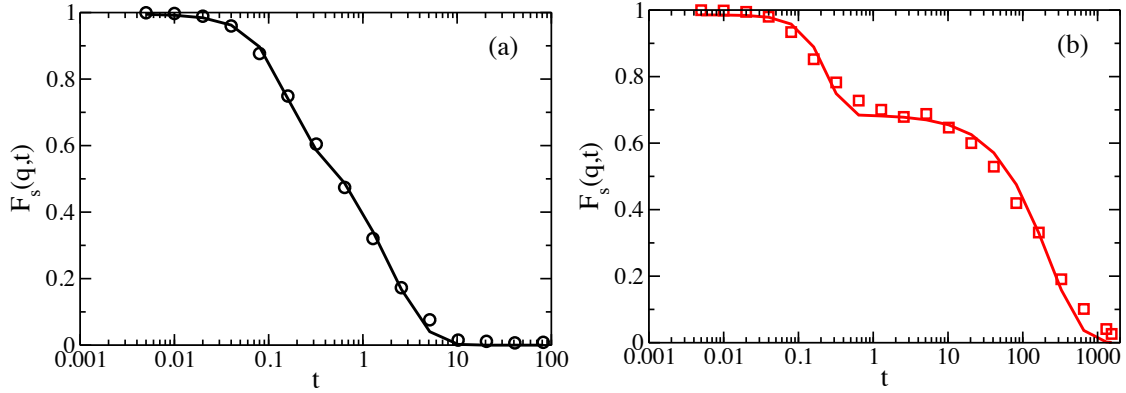


Figure S6. Self intermediate function $F_s(q,t)$ for $T=1.0$ (a) and 0.5 (b). The solid curves are the ones fitted by Eq.S3.

The quality of the fit is measured by the correlation coefficient ε between the fitted curves and the intermediate scattering function $F_s(q_1,t)$. What we would like to establish is how ε varies with the value of h . To estimate the uncertainty in the value of h we have proceeded as follows.

Step 1. Fit the intermediate scattering function $F_s(q_1,t)$ with the Eq.(S3), and let $h=h^*$.

Step 2. Fix $h=h^*+\delta$ and redo the fit over the 2 remaining variables and record the overall measure of the quality ε of the new fit.

Step3. Repeat this for a range of δ 's, +ve and -ve, and plot ε as a function of δ . The result is plotted in Fig. S7. As expected, there is an extremum at $\delta = 0$, i.e. the original fit returned the best value of h . What we are interested in is the curvature about the extremum. If it is high curvature then it means that the uncertainty in the original value of h was small. If the curvature is low, i.e. varying h does not change the quality of fit, then the uncertainty in h is high. The uncertainty in h can be estimated by the interval in δ over which ε lies above some threshold value, here $\varepsilon^* > 0.95$.

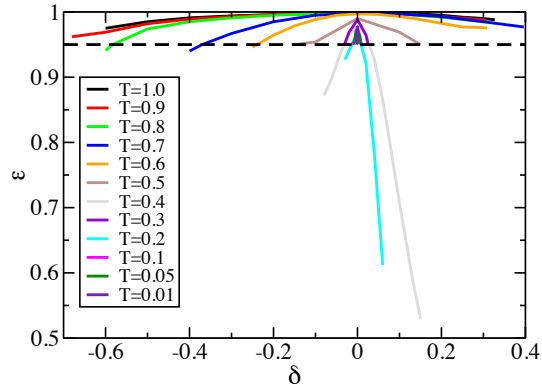


Figure S7. The quality of the fits as a function of δ (explained in the text) for all temperatures in this work. The black dashed line is the threshold value chosen here, $\varepsilon^*=0.95$.

5. The variance of structural restraint degree on cooling of the KA mixture

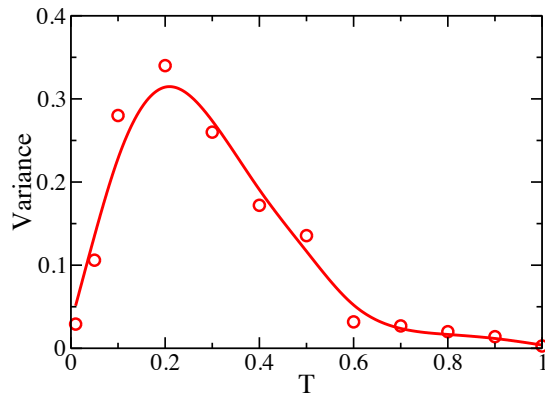


Figure S8. The variance of structural restraint degree (μ) of KA model as the function of temperature on cooling process.